A Geometric Model for Specularity Prediction on Planar Surfaces with Multiple Light Sources

Alexandre Morgand, Mohamed Tamaazousti and Adrien Bartoli

Abstract—Specularities are often problematic in computer vision since they impact the dynamic range of the image intensity. A natural approach would be to predict and discard them using computer graphics models. However, these models depend on parameters which are difficult to estimate (light sources, objects' material properties and camera). We present a geometric model called JOLIMAS: JOint LIght-MAterial Specularity, which predicts the shape of specularities. JOLIMAS is reconstructed from images of specularities observed on a planar surface. It implicitly includes light and material properties, which are intrinsic to specularities. This model was motivated by the observation that specularities have a conic shape on planar surfaces. The conic shape is obtained by projecting a fixed quadric on the planar surface. JOLIMAS thus predicts the specularity using a simple geometric approach with static parameters (object material and light source shape). It is adapted to indoor light sources such as light bulbs and fluorescent lamps. The prediction has been tested on synthetic and real sequences. It works in a multi-light context by reconstructing a quadric for each light source with special cases such as lights being switched on or off. We also used specularity prediction for dynamic retexturing and obtained convincing rendering results. Further results are presented as supplementary video material.

Index Terms—JOLIMAS, Specular Reflection, Multiple Light Sources, Phong, Blinn-Phong, Specularity, Prediction, Retexturing, Quadric, Dual Space, Conic, Real Time.

✦

1 INTRODUCTION

THE photometric phenomenon of specular reflection is often seen in images. Specularities occur on surfaces when their imperfections are smaller than the incident wavelength, making them mirror-like. In that case, light is completely reflected in a specular form (the angles of reflection and incidence are equal with respect to the normal of the surface) creating a specular highlight in the image. Specularities are important in several fields of research. They often saturate the camera response and may thus impact the rest of the image. The strong change of image intensity they induce may disturb computer vision algorithms such as camera localization, tracking and 3D reconstruction. However, instead of treating these specularities as perturbations or outliers, they may be considered as useful primitives. In fact, specularities give additional information about the depth of the scene [12, 38] and may improve camera localization [28,31,41], 3D reconstruction [12,39] and scene material analysis [6, 33, 34, 40]. In Augmented Reality (AR) and computer graphics, specularities significantly improve rendering quality [9,13,14,22,23,26,37,38]. Indeed, it was shown that they play a key role in scene perception by the human brain [1]. To better achieve these applications, specularity prediction for a given viewpoint and scene is tremendously important.

By observing the shape of a specularity on a planar surface, it seems plausible to model it by a conic. This shape is obtained by projecting a quadric on a plane. Considering these elements, it is natural to ask if it would be possible to reconstruct a fixed quadric whose projection would explain the specularity for
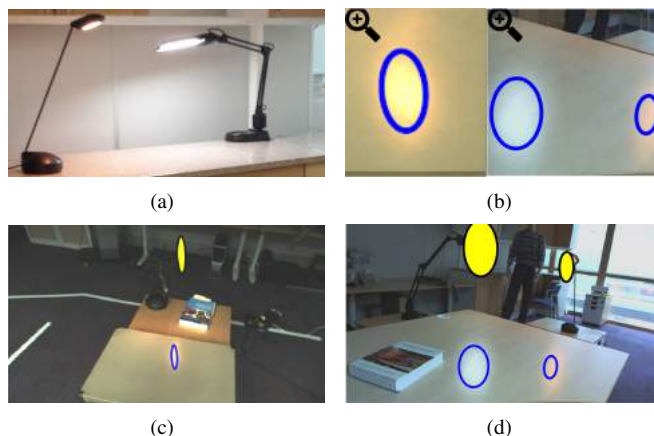
Figure 1: We observe that specularities have a conic shape on planar surfaces. We approximate them by projecting a fixed quadric whose parameters includes light and material properties. This figure presents quadric reconstruction examples (in yellow) for two light types (light bulb and fluorescent lamp) and two materials (steel table (c) and wooden table (d)). Some of the light sources can be seen in (a). Once reconstructed, each quadric can predict future specular reflections by simple perspective projection (blue conics). (b) shows the specularity prediction close-up in the respective sequences: light bulb/steel table (c) and light bulb and fluorescent lamp/wooden table (d).

• *A. Morgand is with CEA,LIST, Gif-sur-Yvette, France and IP-UMR 6602 - CNRS/UCA/CHU, Clermont-Ferrand, France.*
  E-mail: alexandre.morgand@cea.fr
• *M. Tamaazousti is with CEA, LIST.*
  E-mail: mohamed.tamaazousti@cea.fr
• *A. Bartoli is with IP.*
  E-mail: adrien.bartoli@gmail.com

every viewpoint. If possible, this model would represent a link between the photometric phenomenon of specularities (light and material) and multiple view geometry [16]. We propose JOint LIght-MAterial Specularity (JOLIMAS), a geometric model to predict the position and shape of specularities in existing and new viewpoints, as illustrated in figure 1. This model is composed of

a quadric which implicitly captures light and material properties, which are intrinsic to specularities. This quadric is reconstructed from the conics associated with the specularity. We mostly use planar surfaces because they are dominant in the indoor context [5, 22]. With JOLIMAS, we collect experimental evidence to answer the above mentioned modeling hypothesis. It turns out that the shape of specularities can be very well approximated by a purely quadric based model. We consider specularities which are clearly visible (with high intensity) because their impact on computer vision algorithms is high as opposed to fainter specularities. When planar surfaces of strong roughness affect the specularity contours, our conic approximation is still relevant because our model is abstracting this parameter along with the reflectance of the surface material.

JOLIMAS is presented in section 3. Its estimation is detailed in section 4 and especially the quadric reconstruction. We also detail the epipolar correction process used on the input data. Our model is generalized to the multi-light context with multiple specularities in each image in section 4.3. This empirical model, along with specularity prediction, is tested on synthetic and real sequences including bulb and fluorescent lamps in section 5. We present two applications in section 6: the estimation of the dynamic state of light sources (turned on and off) and specularity prediction on real sequences for retexturing with one or several light sources.

2 RELATED WORK

Specularity prediction is a difficult problem. A specularity is a complex photometric phenomenon described by its size, position, shape and intensity. Additionally, these elements are highly influenced by the camera (pose and response function), the scene's geometry and material (reflectance and roughness) and the light sources (position, shape, intensity, isotropicity). There are currently no methods to estimate a predictive specularity model from images. A natural approach would be to estimate a physical model of the scene with the associated parameters for the materials and light sources. As opposed to camera localization and 3D scene geometric reconstruction, the estimation of these parameters is extremely difficult and ill-posed in practice when only a monocular image sequence is available. Existing methods that estimate the light sources can be divided in two categories: global illumination and primary source reconstruction.

For global illumination, Jachnik *et al.* [22] proposed light environment map reconstruction from a video of a planar specular surface. This method uses a GPU implementation and achieves a convincing photo-realistic rendering for AR application. However, the model does not distinguish primary and secondary sources, which is essential for specularity prediction for unknown viewpoints. Meilland *et al.* [30] reconstruct primary sources as point lights. They are directly observed from an RGB-D camera. Despite its high quality rendering, the method lacks flexibility. In fact, the method represents a volumetric light source such as fluorescent light by a set of point lights. Therefore, the method has to compute an intensity for each of the different points which are supposed to represent the same light. Moreover, dynamic light sources (lights changing intensity over time) are not handled and specular materials are not modeled. As a consequence, this method cannot predict specular reflections for new viewpoints.

Solutions have been also proposed to the primary light source reconstruction problem. Ideally, every physical light model has to be associated with a geometry (position and shape), color [29] and

intensity value to realistically match the lighting conditions of the scene. Even though many light models exist in computer graphics, the ones used for light source reconstruction in computer vision are generally divided in two categories: directional light sources and point light sources. Lagger *et al.* [27] describe a method to compute directional lights using specular reflections on a mobile object observed from a fixed viewpoint. This application is limited as due to the view-dependent aspect of specular reflections, light sources should be estimated for each position. Neither shape, position nor object material are taken into account, making the method unable to predict specular reflections. Similar approaches [5,10,24,46] experience the same issues with the same limitations. On point light source estimation, Boom *et al.*'s approach [4] computes a primary light source assuming Lambertian surfaces and using an RGB-D camera. From the diffuse term, by comparing synthesic rendering with the real scene, a point light is estimated. However, this method is not suitable for real-time applications and for volumetric light estimation such as fluorescent lamps. By computing only one light source without its shape and the associated specular material properties, specularity prediction cannot be achieved.

To predict a specularity from physical light source reconstruction, the complex parameters of light and materials have to be computed. In practice, a physical approach as the ones described previously does not seem practical, as we only have an image sequence and camera pose as inputs. To address this challenging highly non-linear problem, we propose a quadric based model reconstructed from conics fitted to specularities on each viewpoint. This empirical model, implicitly capturing the light source and material parameters, facilitates specularity prediction from new viewpoints, even in a multiple light source context.

3 MODELING

We propose JOLIMAS, an empirical model, including light source and material properties. JOLIMAS uses a quadric reconstructed from conics fitted to the specularity for each viewpoint as illustrated in figure 2. We assume that the observed surface is planar and non-Lambertian and that each specularity is associated with a light source. A formal demonstration of our conic specularity approximation on a planar surface is given in the following section. We then evaluate this hypothesis empirically.

3.1 Theoretical Motivation

3.1.1 The Phong Model

We use the Phong illumination model [35] which is the baseline in many BRDF models [20]. JOLIMAS does not use Phong's model for its reconstruction but uses it as theoretical means to derive some of its founding properties. This illumination model divides the image in three components: diffuse, ambient and specular. Recent models such as Blinn-Phong [3], Ward [45], Cook-Torrance [7] differ in the way the specular term is computed. These models propose improved roughness computation. Even if the Phong specular term is no longer used in rendering, it suits the approximation in our study. Indeed, roughness is implicitly included in the proposed JOLIMAS model.

The Phong intensity function of a 3D surface point $\mathbf{P} = \begin{bmatrix} P_X & P_Y & P_Z \end{bmatrix}^\top$ is given by:

$$I(\mathbf{P}) = i_a k_a + i_d k_d (\hat{\mathbf{L}}(\mathbf{P}) \cdot \hat{\mathbf{N}}) + i_s k_s (\hat{\mathbf{R}}(\mathbf{P}) \cdot \hat{\mathbf{V}}(\mathbf{P}))^n, \qquad (1)$$
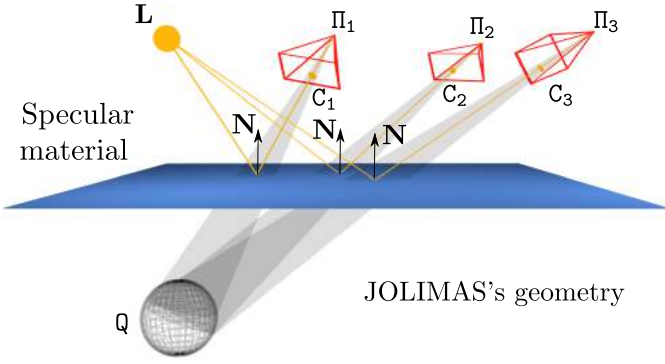
Figure 2: Illustration of JOLIMAS, showing the link between photometry (light and surface material) and multiple view geometry (our geometric model). The light source $\mathbf{L}$, which could be either a light bulb or a fluorescent lamp, creates specularities (the yellow conics) in the different viewpoints Π_1, Π_2 and Π_3 with Π composed of the rotation matrix R_{rot} and position $\mathbf{V}$. From multiple viewpoints, a quadric $\mathbb{Q}$ is reconstructed from specular reflections of conic shape $\mathbb{C}_1$, $\mathbb{C}_2$ and $\mathbb{C}_3$ in the images. We then use the quadric $\mathbb{Q}$ projected onto the planar surface to predict specularities from new viewpoints.

with $\hat{\mathbf{R}}(\mathbf{P}) = -\mu(\mathbf{R} - \mathbf{P})$ the normalized direction of a perfectly reflected ray of the light source $\mathbf{L} = \begin{bmatrix} L_X & L_Y & L_Z \end{bmatrix}^\top$ such that $\mathbf{R} = \begin{bmatrix} L_X & L_Y & -L_Z \end{bmatrix}^\top$, $\hat{\mathbf{L}}$ and $\hat{\mathbf{V}}$ the normalized direction pointing towards the light source $\mathbf{L}$ and the viewer $\mathbf{V} = \begin{bmatrix} V_X & V_Y & V_Z \end{bmatrix}^\top$. We use the notation $\hat{\ }$ to indicate a normalized vector such that $\hat{\mathbf{L}}(\mathbf{P}) = \mu(\mathbf{L} - \mathbf{P})$ and $\hat{\mathbf{V}}(\mathbf{P}) = \mu(\mathbf{V} - \mathbf{P})$ with μ the normalization operator:

$$\mu(\mathbf{A}) = \frac{\mathbf{A}}{||\mathbf{A}||}.$$

n represents the glossiness of the surface, k_s, k_a and k_d the ratios of reflection of the specular, ambient and diffuse terms of the incoming light, $\hat{\mathbf{N}}$ the normal of the surface S and i_s, i_a and i_d the incoming intensities on the surface for the specular, ambient and diffuse terms. We choose the world coordinate frame so that the scene's flat surface $S \subset \mathbb{R}^3$ is the $(\mathbf{XY})$ plane. In other words, $S = \{\mathbf{P} \in \mathbb{R}^3 | P_Z = 0\}$. We can thus parameterize S by a point $\mathbf{p} \in \mathbb{R}^2$ and define $\mathbf{P} = \begin{bmatrix} P_X & P_Y & P_Z \end{bmatrix}^\top$.

3.1.2   Specular Term
At point $\mathbf{P}$, the specular component I_s is given by:

$$I_s(\mathbf{P}) = i_s k_s (\hat{\mathbf{R}}(\mathbf{P}) \cdot \hat{\mathbf{V}}(\mathbf{P}))^n, \tag{2}$$

We want to analyze the isocontours of a specular highlight on the surface S for a viewpoint $\mathbf{V}$, a light source $\mathbf{L}$ and direction $\mathbf{R}$. We start by relaxing the highlight model to the following simpler model:

$$\tilde{I}_s(\mathbf{P}) = -\mu(\mathbf{R} - \mathbf{P})^\top \mu(\mathbf{V} - \mathbf{P}). \tag{3}$$

We first expand equation (3) for a general intensity (in gray scale) τ and then solve it for $\tau = 1$ and $\tau = 0$:

$$\tilde{I}_s(\mathbf{P}) = \tau. \tag{4}$$

Because $\tilde{I}_s$ is a scalar product between two normalized vectors, we have $-1 \le \tilde{I}_s \le 1$. Moreover, because $P_Z = 0$, $L_Z > 0$ and $V_Z > 0$, $\tilde{I}_s > 0$. Overall, $0 < \tilde{I}_s \le 1$. By multiplying equation (4) by

$||\mathbf{R} - \mathbf{P}|| ||\mathbf{V} - \mathbf{P}||$, squaring both sides and substracting the right-hand side, we obtain a bivariate quartic (in P_X and P_Y):

$$\left((\mathbf{R} - \mathbf{P})^\top (\mathbf{V} - \mathbf{P})\right)^2 - \tau^2 ||\mathbf{R} - \mathbf{P}||^2 ||\mathbf{V} - \mathbf{P}||^2 = 0.$$

By expanding and collecting the monomials of same degrees, we have:

$$(d^\circ 4)\ (1 - \tau^2)||\mathbf{P}||^4$$
$$(d^\circ 3)\ 2(\tau^2 - 1)(\mathbf{R} + \mathbf{V})^\top \mathbf{P} ||\mathbf{P}||^2$$
$$(d^\circ 2)\ \mathbf{P}^\top (\mathbf{R}\mathbf{R}^\top + 2\tau(1 - 2\tau^2)\mathbf{R}\mathbf{V}^\top +$$
$$(2\mathbf{R}^\top \mathbf{V} - \tau^2 ||\mathbf{R}||^2 - \tau^2 ||\mathbf{V}||^2)\mathtt{I})\mathbf{P}$$
$$(d^\circ 1)\ 2(-\mathbf{R}^\top \mathbf{V}\mathbf{R}^\top - \mathbf{R}^\top \mathbf{V}\mathbf{V}^\top +$$
$$\tau^2 ||\mathbf{R}||^2 \mathbf{V}^\top + \tau^2 ||\mathbf{V}||^2 \mathbf{R}^\top)\mathbf{P}$$
$$(d^\circ 0)\ (\mathbf{R}^\top \mathbf{V})^2 - \tau^2 ||\mathbf{R}||^2 ||\mathbf{V}||^2.$$

We observe that the sum of degrees 3 and 4 factors as:

$$(1 - \tau^2)||\mathbf{P}||^2 \mathbf{P}^\top (\mathbf{P} - 2\mathbf{R} - 2\mathbf{V}). \tag{5}$$

3.1.3   The Brightest Point
For the highest intensity value $\tau = 1$, the monomials of degrees 3 and 4 vanish. The remaining terms form a quadratic equation which can be rewritten as:

$$\tilde{\mathbf{P}}^\top \mathtt{J}\tilde{\mathbf{P}} = 0, \tag{6}$$

where $\tilde{\mathbf{P}} \overset{\text{def}}{=} \begin{bmatrix} \mathbf{P} & 1 \end{bmatrix}^\top$ are the homogeneous coordinates of $\mathbf{P}$. Matrix $\mathtt{J} \in \mathbb{R}^{4 \times 4}$ is symmetric and defined by:

$$\mathtt{J} = \begin{bmatrix} [\mathbf{R} - \mathbf{V}]_\times^2 & [\mathbf{V} \times \mathbf{R}]_\times (\mathbf{V} - \mathbf{R}) \\ ([\mathbf{V} \times \mathbf{R}]_\times (\mathbf{V} - \mathbf{R}))^\top & (\mathbf{R}^\top \mathbf{V})^2 - ||\mathbf{R}||^2 ||\mathbf{V}||^2 \end{bmatrix}$$

We show in appendix B that $\text{rank}(\mathtt{J}) = 2$ and $\mathtt{J}$ is non-negative. This means that $\mathtt{J}$ is a point quadric representing the line containing $\mathbf{R}$ and $\mathbf{V}$. Its intersection with S is defined as the brightest point of the specularity. Consequently, the specularity has a single and well-defined brightest point.

3.1.4   The Outer Contour
The lowest intensity value $\tau = 0$ reveals the nature of the outer contour. Expanding the quartic, we obtain:

$$||\mathbf{P}||^2 - (\mathbf{R} + \mathbf{V})^\top \mathbf{P} + \mathbf{R}^\top \mathbf{V} = 0, \tag{7}$$

which corresponds to a quadric, and more particularly a sphere, whose point matrix is:

$$\mathtt{J} = \begin{bmatrix} \mathtt{I}_3 & -\frac{1}{2}(\mathbf{R} + \mathbf{V}) \\ -\frac{1}{2}(\mathbf{R} + \mathbf{V})^\top & \mathbf{R}^\top \mathbf{V} \end{bmatrix}. \tag{8}$$

By defining the orthographic projection on S as:

$$\mathtt{A} = \begin{bmatrix} 1 & 0 & 0 \\ 0 & 1 & 0 \\ 0 & 0 & 0 \\ 0 & 0 & 1 \end{bmatrix}, \tag{9}$$

the highlight's outer ring is thus given by the conic:

$$\mathtt{C} = \mathtt{A}^\top \mathtt{J}\mathtt{A} = \begin{bmatrix} \mathtt{I}_2 & -\frac{1}{2}(\bar{\mathbf{R}} + \bar{\mathbf{V}}) \\ -\frac{1}{2}(\bar{\mathbf{R}} + \bar{\mathbf{V}})^\top & \mathbf{R}^\top \mathbf{V} \end{bmatrix},$$

with $\bar{\mathbf{R}} \overset{\text{def}}{=} \begin{bmatrix} R_X & R_Y \end{bmatrix}^\top$ and $\bar{\mathbf{V}} \overset{\text{def}}{=} \begin{bmatrix} V_X & V_Y \end{bmatrix}^\top$ the orthographic projection of $\mathbf{R}$ and $\mathbf{V}$ on S respectively. $\mathtt{C}$ represents a real circle for $\tau = 0$. By observing the circle $\mathtt{C}$ into the image plane of the camera of optical center $\mathbf{V}$, an ellipse is obtained.

3.1.5 The Inner Isocontours

To study the inner isocontours which correspond to an arbitrary $\tau \in]0, 1[$, specular reflections could be approximated by conics using the Phong model, as illustrated in figure 3(a) for a point light source and 3(c) for an extended light source. This approximation was also tested and validated with the Blinn-Phong [3] model, as illustrated in figure 3(b) for point a light source and 3(d) for an extended light source. Initially this model was defined as an approximation of the Phong model. It is now often presented by the computer graphics community as more physically accurate than Phong's model and commonly used in computer graphics. This model is physically better because it verifies the Helmholtz equation [15].

(a) Phong, point light   (b) Blinn-Phong, point light

(c) Phong, extended light   (d) Blinn-Phong, extended light
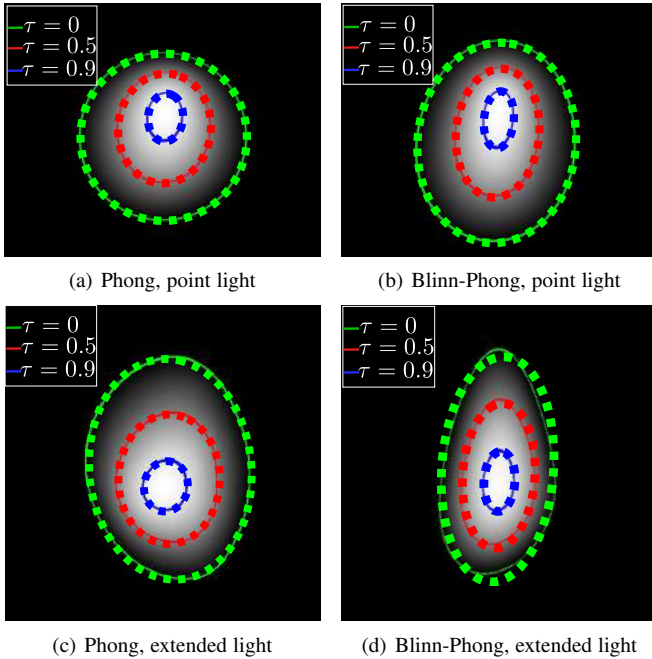
Figure 3: Illustration of our hypothesis of conic shaped specularities for point and extended light sources. A specularity is generated from the specular term of the Phong reflection model in (a) for a simple point light source, and in (c) for an extended light source (a line composed of several point light sources) and from the specular term of the Blinn-Phong reflection model in (b) for a simple point light source and in (d) for an extended light source. Specularities are clearly elliptical in all cases. By observing these shapes in the image plane of the camera, ellipses are obtained. We show in these examples the different isocontours associated to a specific intensity $\tau \in \{0, 0.5, 0.9\}$ (line contours in green, red and blue) along with the fitted conics (in dotted contours in green, red and blue). Our hypothesis of conic shaped specularity is clearly valid in these examples.

3.2 Empirical Validation from Simulated Data

To validate our conic approximation of specularities, we use the method of Fitzgibbon *et al.* [11] for ellipse fitting on different values of $\tau \in [0, 1]$ on the specular term alone and on the combined diffuse and specular terms. In an AR context, the diffuse and specular terms are correlated. To compute our synthetic data, we generated $2,000 \times 2,000$ images using the Phong [35] and Blinn-Phong [3] local illumination models using a random position of the light source and camera above a planar surface with fixed size. The

goal is to analyze the shape of the specularity for a fixed intensity $\tau \in [0, 1]$. For each value of τ, with a step of 0.05 between each value, we run 1,000 scenarios of different light sources and camera poses. The error is computed using the distance from Sturm *et al.* [42] between the fitted conic and the isocontours for each scenario. The specular and diffuse terms are generated using the Phong and Blinn-Phong illumination models. The empirical validation of our conic approximation is given in figure 4(a) for point light sources and in figure 4(b) for extended light sources. In computer graphics, an extended light source can be represented as a set of point light sources, *e.g* a line for fluorescent lamps.

(a) Point light
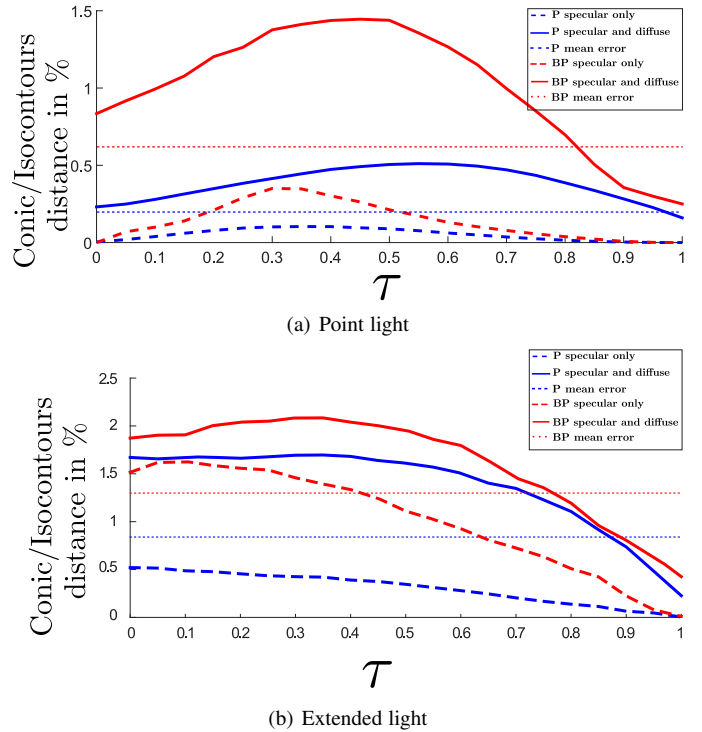
(b) Extended light

Figure 4: Empirical validation from simulated data on (a) point light sources and (b) extended light sources. Our hypothesis of conic shaped specularity is tested on the Phong (P) and the Blinn-Phong (BP) illumination models for different values of intensity $\tau \in [0, 1]$. This hypothesis is tested for the specular term alone and for the combination of the specular and diffuse terms.

The error is computed as a ratio of the geometric distance with the diameter of the conic in pixels for $\tau = 0$. The results show our approximation fits synthetic data with a mean error of 0.2% and 0.6% for the Phong and Blinn-Phong models for a point light source and a mean error of 0.7% and 1.3% for the Phong and Blinn-Phong models for an extended light source (a combination of several point light sources). These results confirm our conic representation to be reliable and accurate for point and extended light sources. For extended light sources such as fluorescent lamps, our conic shaped specularity approximation is still relevant, as shown in figure 4(b). We empirically show that a fixed unique quadric exists for multiple viewpoints that explains the conics in section 5.1.

4 MODEL ESTIMATION

We showed that the shape of a specularity on a plane surface could be approximated by a conic. The main contribution of our

method is an empirical model for specularity prediction modeled by a quadric Q associated with its projections on the plane S for a given camera pose $\Pi = \begin{bmatrix} R_{rot} & V \end{bmatrix}$.

4.1 Overview

The pipeline of the proposed method is as follows:

- Specularity detection in images [32]
- Conic fitting to specularities [11]
- Quadric reconstruction [8]
- Specularity prediction by quadric projection

Our specularity detection process follows the implementation of Morgand *et al.* [32]. This method is divided in three steps. First, a pre-processing to handle image noise and the dynamic lighting context; then, an automatic thresholding process is conducted based on an empirical value of brightness. To further filter misdetections, the method uses an intensity gradient criterion to discriminate specular surfaces from misdetected white textures. This method assumes that the intensity inside the specularity is isotropic and decreasing from the brightest point. The conic fitting process uses the binary image outputed by the specularity detection process to provide the input conics for the quadric reconstruction.

4.2 Quadric Reconstruction

4.2.1 Linear Formulation

We use the approach of Cross *et al.* [8] which reconstructs a dual quadric Q^* from several dual conics C^* in closed form by vectorizing the linear relationship:

$$\Pi Q^* \Pi^\top = C^*. \tag{10}$$

The vectorization of equation (10) is given in appendix A. By vectorizing Q^* and C^* as $\mathbf{Q}_v^*$ and $\mathbf{C}_v^*$, we build equation (11), equivalent to using specular reflections as conics C and JOLIMAS as the quadric Q for n viewpoints with $n \geq 3$. The system is $Mw = 0$, with:

$$\underbrace{\begin{pmatrix} B_1 & -\mathbf{C}_{1,v}^* & 0 & \dots & 0 \\ B_2 & 0 & -\mathbf{C}_{2,v}^* & & 0 \\ \vdots & 0 & 0 & \ddots & \vdots \\ B_n & 0 & 0 & \dots & -\mathbf{C}_{n,v}^* \end{pmatrix}}_{M} \underbrace{\begin{pmatrix} \mathbf{Q}_v^* \\ \alpha_1 \\ \alpha_2 \\ \vdots \\ \alpha_n \end{pmatrix}}_{w} = 0, \tag{11}$$

with $B_i \in \mathbb{R}^{6 \times 10}$. The solutions of system (11) are retrieved by a singular value decomposition (SVD) of M. Note that α_i corresponds to a scale such that $\alpha_i \mathbf{C}_{i,v}^* = B_i \mathbf{Q}_{i,v}^*$ for the viewpoint i. The quadric reconstruction process is illustrated in figure 2. However, system (11) is sensitive to the fitting errors of the input conics. To ensure the quality of the input conics used for the reconstruction, we use epipolar correction for the input conics. This correction ensure that the conics respect the epipolar constraint for the quadric initialization process. To further improve the quadric reconstruction, a non-linear refinement process is proposed.

4.2.2 Epipolar Correction for Conics Outlines

Quadric reconstruction from specular reflections is not an easy task. Indeed, as opposed to Cross *et al.* [8], our reconstruction is done using specular reflection observations in several images instead of direct object observations.

In Cross *et al.*'s approach, conic fitting is less prone to errors. Indeed, specular reflections represent semi-mirror images of light sources reflected on specular surfaces. These specularities have contours which are not perfectly consistent due to their intensity variation between images causing the fitted conics to be epipolar inconsistent, as shown in figure 5. This drawback could affect

(a)

(b)   (c)
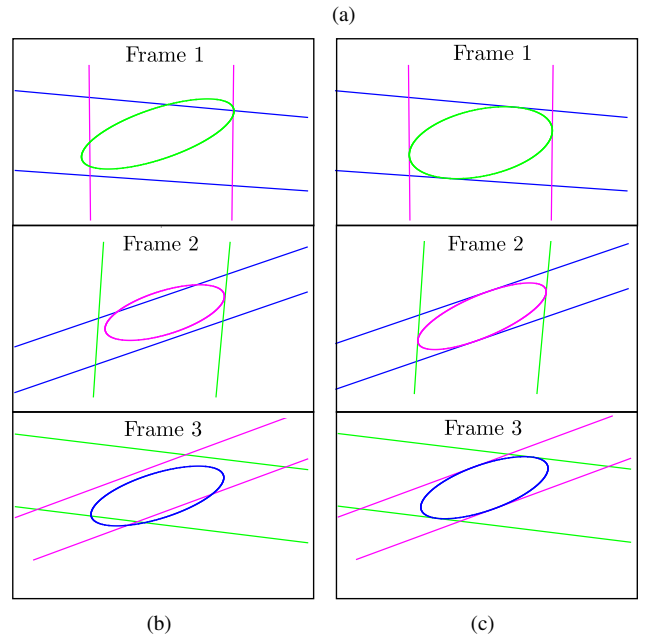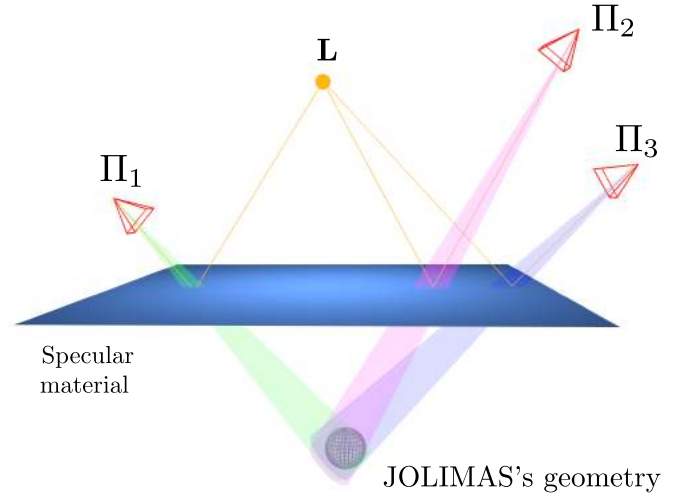
Figure 5: Epipolar lines of the conics for three camera poses Π_1, Π_2 and Π_3 and a light source L. The scene is showed in (a) and the associated conics and epipolar lines are in (b). In the naive form, the epipolar geometry of the conics is not respected. This results in an incorrect quadric reconstruction and will cause an incorrect specularity prediction. Epipolar correction fixes this issue by correcting the conics to fit the epipolar constraints without drastically changing the shape.

the quality of the quadric reconstruction from specularities. As a result, epipolar consistency should be checked on every view of the initialization to optimize the result. Without corresponding conic outlines, the linear system (11) could return incoherent results. The dual space allows an elegant formulation of the problem, but because of the algebraic nature of the equations, a small amount of noise may cause large errors in the estimated quadric.

A conic is uniquely defined from 5 non-aligned points or 5 non-colinear lines in the dual space. For three viewpoints, each conic is constrained by two pairs of lines coming from the other viewpoints, making the estimation problem of the dual conic under-constraint. One of the proposed solutions of Reyes et al. [36] is to estimate more accurate epipolar lines from conics in the other images and an additional line from the tangent of a contour point of the conic in the current image. Using these 5 lines, we compute a unique dual conic. This process is repeated for each contour point and for each viewpoint. The corrected conic is the one minimizing the Conic/Point distance of Sturm et al. [42]. Note that the efficiency of the fitting will strongly depend on the quality of the specularity contour points. The resulting conics for each viewpoints will be used in the the reconstruction process as they respect the epipolar constraints. This process is iterative, reliable and efficient. We illustrate a step of the process in figure 6. In our context, we cannot limit the reconstruction to only three viewpoints. We thus include a non-linear refinement process on 3+ viewpoints to improve the quadric reconstruction.
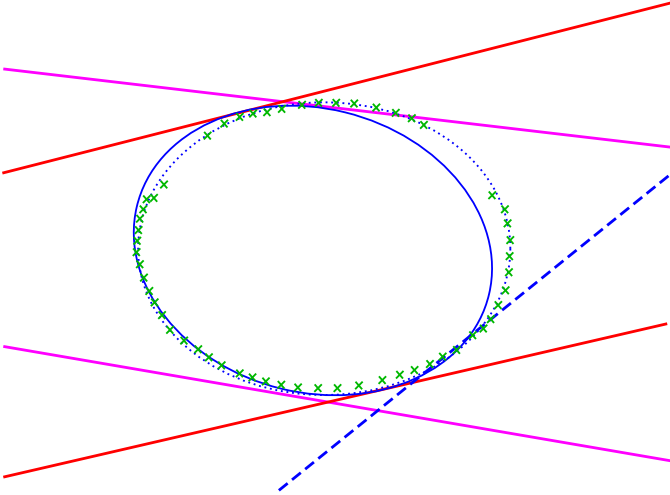
Figure 6: Epipolar correction of Reyes et al. [36]. The observed conic (blue dots) is computed from the contour points (dark crosses) of the specularity. The four epipolar lines created from the other viewpoints are represented in red and magenta. To estimate the dual conic respecting the epipolar geometry, a fifth line computed from the tangent of one of the contour point (dotted line in blue). We compute a conic in the dual space for every contour point and choose the one (represented here) minimizing the distance Conic/Point of Sturm et al. [42] for each of the three viewpoints. The resulting conics will be used to reconstruct an accurate quadric from epipolar consistent conics.

4.2.3   Non-linear Refinement

Non-linear refinement is crucial to handle noisy inputs and to correct the initialization on a wider range of viewpoints. For real

data, the initialization process is not sufficient. Our context differs from Cross et al.'s [8] due to the noisy aspect of a specular reflection, adding a modeling problem. In fact, a specularity contour is not easily approximated due to its dependency to the camera parameters, material properties and illumination conditions. To further improve the initialization, the quadric reconstruction of Reyes et al.'s [36] also includes a non-linear refinement process minimizing the Conic-Point distance [42] between the quadric projections for each viewpoint and the associated contours. This method gives us a robust reconstruction of the quadric for 3+ viewpoints in real-time and usable for specularity prediction on unknown viewpoints. For these advantages, we used Reyes et al.'s method [36] for the epipolar correction, initialization and we use a similar cost function.

To further constrain the refinement and reduce the dimensionality of the minimization, latent variables are used as 2D points noted $\mathbf{q}'_{i,j}$ constrained to be on the conic section C and compared with the specularities contour points $\mathbf{q}_{i,j}$. This formulation allows us to set the following constraint during the minimization:

$$\mathbf{q}'^{\top}_{i,j}\mathsf{C}_j\mathbf{q}'_{i,j} = 0. \tag{12}$$

The parameters of our minimization is the matrix representation of Q along with the different points constrained on the conic section. Before the refinement process, these latent variables $\mathbf{q}'_{i,j}$ are estimated by the conic parameterization of [42] for each conic C_j of index j. The cost function with latent variables is:

$$\begin{cases} \min\limits_{\mathsf{Q},\mathbf{q}'_{1,1},...,\mathbf{q}'_{n,m_n}} & \sum\limits_{i=1}^{n}\sum\limits_{j=1}^{m_i} d(\mathbf{q}'_{i,j},\mathbf{q}_{i,j})^2, \\ \text{subject to} & \mathbf{q}'^{\top}_{i,j}\mathsf{C}_j\mathbf{q}'_{i,j} = 0 \end{cases} \tag{13}$$

4.3   JOLIMAS in a Multiple Light Context

An additional feature of our model is to be able to predict several specularities from distinct light sources. Indeed, on planar surfaces, a specular reflection is associated with only one light source. By labeling and tracking these cues, several quadrics are reconstructed together. After our specularity detection process, we thus track each specular reflection throughout the video stream. Tracking specularities is essential to count and discriminate the light sources. Our tracking is achieved by computing the evolution of the specular reflection contours from an image to the next by detecting intersections between the contour of the current frame and the previous one, as illustrated in figure 7. Even for large camera motion, specularities naturally follow the camera motion (especially for planar surfaces), allowing our algorithm to be robust for complexes cases. This tracking is done on every frame using Suzuki et al.'s [43] contour detection algorithm to have accurate contours extracted from the binary image output by our specularity detection method in real time. However, keeping track of overlapping specularities (when two light sources have the same direction towards the viewpoint) is yet to be achieved by our method, although these cases remain rare. For overexposed images, the method of Morgand et al. [32] that we use for specularity detection may confuse white bright textures with specularities. To ensure a robust specularity detection, a multi-view process on the specular candidates is mandatory. In fact, as opposed to the 3D contours of a texture, the 3D contours of the specularity are moving on the 3D surface when the camera is moving as well. By computing the homography between two frames, the specular

candidates can be warped. If the contours are very similar, the candidate is a texture, and a specularity otherwise.

(a) (b)

(c) (d)
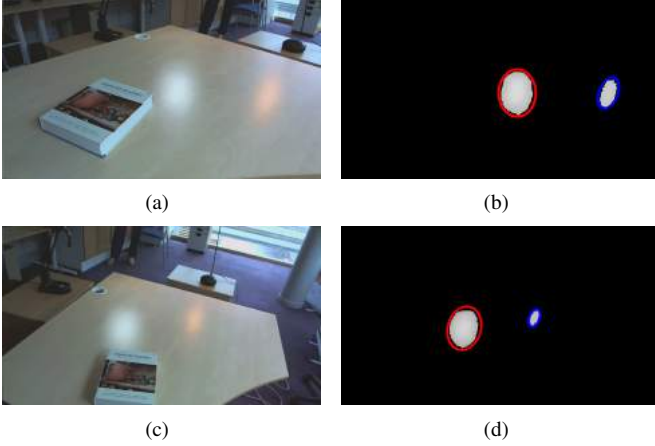
Figure 7: Multi-light labeling and tracking of specularities (in blue and red). (a) and (c) represent two viewpoints on a wooden table. (b) and (d) represent the fitted conics associated with each light source (in blue and red).

5 EXPERIMENTAL RESULTS

To evaluate the relevance and accuracy of our proposed parametric light source model, two experiments are conducted. We first analyze the performance of JOLIMAS for specularity prediction on synthetic data generated from the Phong and Blinn-Phong illumination models. Thereafter, this prediction ability is evaluated on five real sequences including different light source types such as bulb and fluorescent lamps.

5.1 Synthetic Data

We give a synthetic validation of our quadric approximation in JOLIMAS. The simulated camera has a $50mm$ lens with a centered principal point. The images have $0.45 \times 0.45mm$ pixels for a resolution of $1,000 \times 1,000$. Our scene is composed of a $20 \times 20cm$ specular plane and we observe a moving specularity. We randomly select viewpoints and a light source above the plane. From the Phong and Blinn-Phong illumination models, for each $\tau \in [0,1]$, 100 quadric estimations are made using 100 viewpoints. We compute the geometric distance between the observed specularity in the image (which combines the diffuse and specular terms in real data) with the associated quadric projection to the viewpoint.

As shown in figure 8, our quadric approximation is efficient in producing accurate specularity predictions for $\tau \in [0,1]$ for both the Phong and Blinn-Phong illumination models with respectively 0.3% and 0.45% error on average, relative to the scene dimension. This experiment was also conducted on an extended light source composed of several point light sources for the Phong and Blinn-Phong models for an average error of 1% and 1.6% respectively. However, the refinement process does not play a significant role on synthetic sequences, where the conditions are ideal.

5.2 Real Data

We evaluate JOLIMAS on real sequences with three different light sources and five different materials. The quadric is reconstructed

(a) Point light
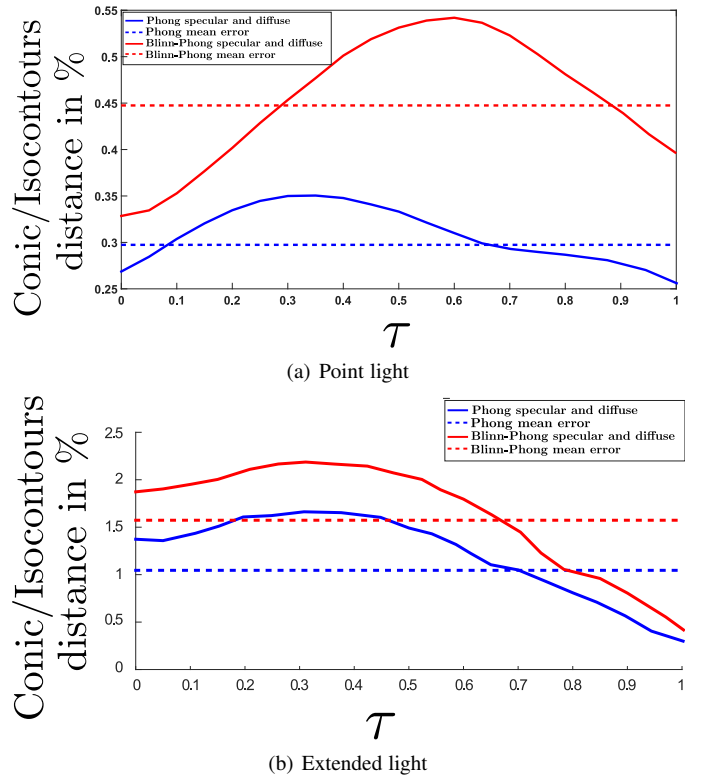
(b) Extended light

Figure 8: Validation of our model by measuring the prediction error on synthetic data for a point light (a) and an extended light source (b). From 100 viewpoints, a fixed quadric is reconstructed and its projection is compared to specularity contours of each viewpoint using Sturm *et al.*'s [42] distance. This error is normalized according to the scene dimension.

from conics fitted by the method of Fitzgibbon *et al.* [11]. The specularities are detected using the approach of Morgand *et al.* [32]. Camera poses are computed using a SLAM method [44]. The reconstruction process is composed of real-time methods and the prediction is done also in real-time by simply projecting the reconstructed quadric. The accuracy of our quadric model is evaluated on real data to quantify the prediction ability of our approach. We use the distance of Sturm *et al.* [42] to measure the Conic-Contour distance to the ground truth. To retrieve ground truth, we manually select the specularities on the different sequences with light bulbs and fluorescent lamps. Our results are given in table 1, figure 1 and figure 9.

In our context, the quadric initialization is not sufficient on its own to predict the specularities accurately. Estimating reliable specularity contours is difficult in practice which highly impacts the quadric reconstruction quality. Adding an epipolar correction to the outlines of the input conics provides better results. By combining the epipolar correction with the non-linear refinement, we achieve a maximum error value of 62.8 pixels. For real sequences, JOLIMAS is accurate and allows specularity prediction from new viewpoints for a variety of light sources in real-time.

6 SPECULARITY PREDICTION'S APPLICATIONS

6.1 Detecting a Light's On/Off State

We address the question of specularity analysis by comparing the specularity detection and prediction. This analysis has several

Table 1: Empirical validation of our model and its capacity to predict specular reflections in images for 5 real sequences presented in figures 1 and 9 . The average error of prediction per specularity is computed in pixels using Sturm *et al.*'s distance [42] between the predicted conics and the detected specularity contours. This prediction is evaluated at three steps: initialization, epipolar correction and non-linear refinement. We observe a significant decrease of the cost at each step.

2D distance (in pixels) / Sequence	Initialization	Epipolar correction	Non-linear refinement
Light bulb 1 Steel table	110.3	82.2	62.8
Fluorescent lamp Whiteboard	210.6	80.9	31.6
Light bulb 2 Plastic book	85.2	66.7	28.9
Light bulb 1 + fluorescent lamp Wooden table	162.1	96.9	40.1
Light bulb 1, 2 + fluorescent lamp Kitchen counter	240.3	144.9	60.3

interests:

- If the conics associated respectively with the prediction and the detection have the same shape but a different position, the camera pose is not accurate enough.
- If the conics associated respectively with the prediction and the detection have the same position but not the same scale, the light source intensity has changed.
- If the conic associated to the detection is missing, the light source is turned off or occluded.

This last feature will be used in this section. Several applications such as retexturing and diminished reality are disturbed by light sources with changing states (on/off) because this creates an increase or a decrease of the intensity in the image. Moreover, the camera needs to adjust to the new lighting context, which will affect the results. Currently, no solution is proposed to resolve this issue. By using the JOLIMAS specularity prediction, we can track a light source even if turned off or on by comparing the specularity prediction with the detection. We test the ability of the model to predict light with changing state (on/off) in figure 9(d) on the sequence already presented. In this sequence, three light sources are used (two light bulbs and one fluorescent lamp) on a plastic kitchen counter. We turn on and off each light source individually before switching off all light sources at the end of the sequence. This is illustrated in figure 10. The results presented in this sequence enable us to detect fast changing light states such as the flickering of the fluorescent lamp when turned on in a multi-light context.

6.2 Dynamic Retexturing

It was shown that the human brain takes into account the specularities to understand a scene [1]. Therefore, specularity rendering could greatly improve the following applications:

- Retexturing for augmented reality
- Diminished reality when a specularity is crossing the area to inpaint [19, 25]
- Virtual viewpoint prediction (where the camera physically never went)

(a)

(b)

(c)

(d)
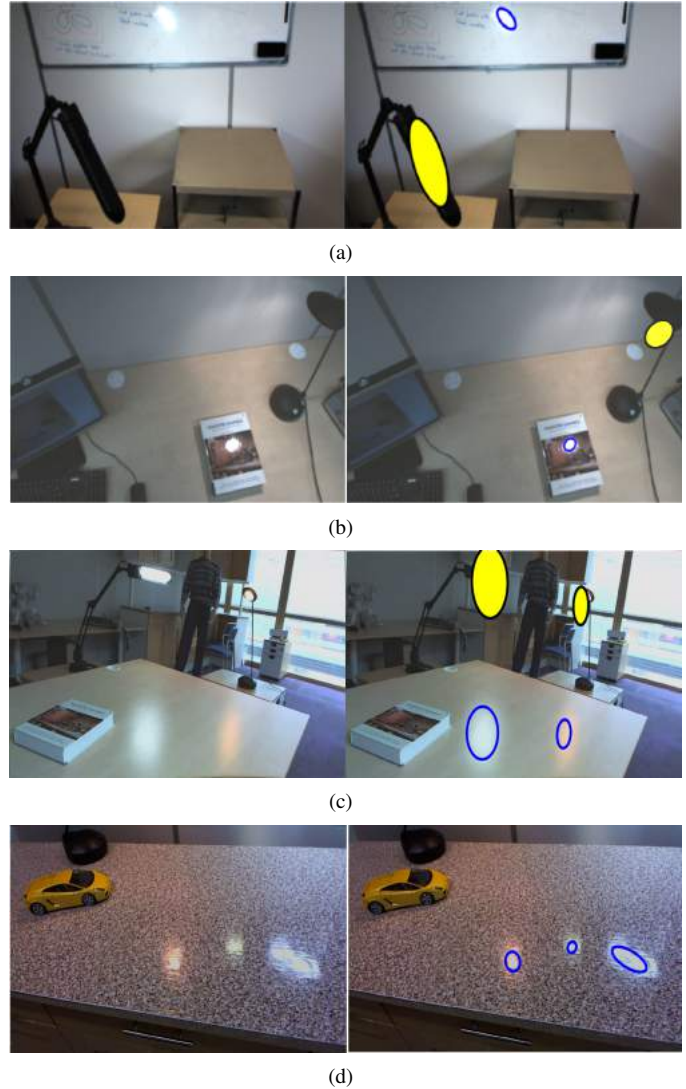
Figure 9: Specularity prediction on four real sequences. In (a) a whiteboard illuminated by a fluorescent lamp, in (b) a book illuminated by a light bulb, in (c) a wooden table illuminated by both spot and fluorescent light sources and in (d) a kitchen counter illuminated by two light bulbs and one fluorescent lamp. Our virtual model is projected on the different planes to fit the observed specularity (blue ellipses). We compute the symmetric from the planes (whiteboard, electronic box and book cover) to display the reconstructed quadric in JOLIMAS (in yellow), which happens to lie on the light sources.

For all these applications, if one wants to render a specularity in the image, one could consider using only the detected specularities in the image and apply them directly on the new texture. However, due to the difficulty of the specularity detection process, this solution does not seem optimal due to unwanted jittering and temporal incoherence affecting the rendering, as shown in figure 11. Indeed, the quality of specularity detection cannot be guaranteed for every viewpoint because of light condition changes, specularity detector limitations, imperfections on the planar surface (roughness) and occluding objects in the scene. The temporal coherence of the rendering is important for applications such as diminished reality [19, 25].

(a)   (b)

(c)   (d)
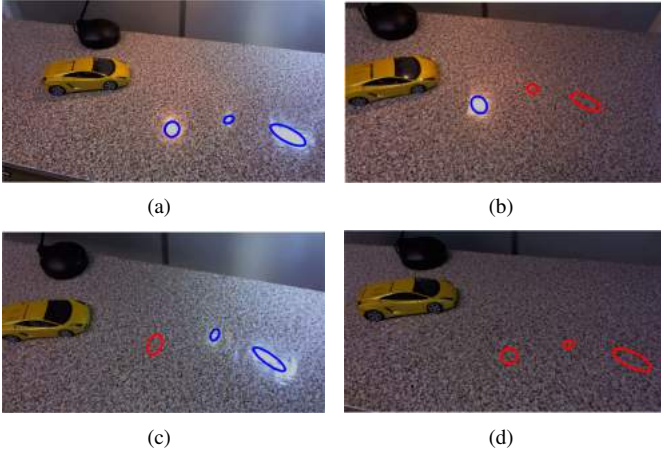
Figure 10: Changing state handling in a multi-light context. The predicted specularities are represented as blue conics when the light sources are on and red conics otherwise. The first light bulb is switched off in (a) and the fluorescent lamp in (b). In (c) the first light bulb and fluorescent lamp are on and the second light bulb is switched off before being switched on. In (d), every light sources are switched off until the end of the sequence.

In this context, the JOLIMAS model, by predicting the specularity using the projection of the quadric from the actual viewpoint is a natural solution to ensure the temporal coherence of the rendering. To achieve the specularity rendering from JOLIMAS, an intensity function describing the intensity variation within the specularity is needed. We propose an approximation based on a 2D Gaussian function. Indeed, a specularity is described as a high intensity area. Starting from the center of this specularity, the intensity is progressively decreased by making use of a Gaussian function. The Gaussian intensity function captures the following properties of the specularity: smooth variation of the intensity and ellipticity of the isocontours, as detailed in section 3.1. The smooth property of the specularity has already been exploited by Kim *et al.* to separate specular and diffuse reflections in an image [21].

Our retexturing method is divided in three steps. Firstly, from detected specularities in the sequence, a mean of the specularity color is computed to fit the lighting conditions. The appropriate Gaussian function is computed on the red, green and blue color channels to match the specularity detected in the sequences. To correctly draw our synthetic specularity on the texture associated to the plane, two homographies are computed: H_2, the transformation from the texture to the planar surface and H_1 transforming the unit circle into the predicted conic (the conic is first transformed by H_2^{-1}). Our synthetic texture replaces the scene planar surface by merging the texture with our Gaussian texture using H_1 and transforms the fusion onto the plane using H_2. Four results of retexturing are shown in figure 12. Due to the lack of geometric modeling of specularity such as ours, we additionally implemented Buteau *et al.* 's approach [5] as baseline method for our retexturing. This recent method reconstructs point light sources from specularities on planar images, making it the closest approach to ours. To achieve retexturing for point light sources, we manually compute every Phong's parameters (roughness, intensity and color of the light sources) and apply only the specular part onto the new texture. As seen in figure 12, our approach accurately matches the intensity, shape and position of the specularities as opposed to [5]

(a)   (b)

(c)
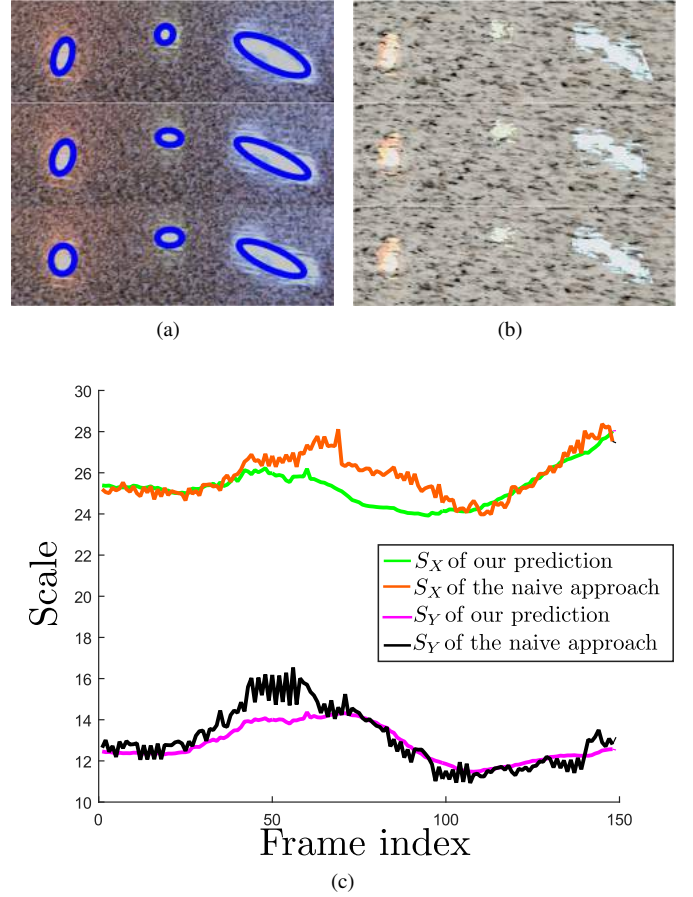
Figure 11: Temporal incoherences on naive conic fitting and retexturing on the multi-light sequence presented in figure 9(d) for three consecutive frames (one frame per row of (a) and (b)). In (a), the jittering of the conic fitting is visible on every specularity when we directly fit ellipses to the specularity detection. This jittering is highlighted in (c) by measuring the evolution of the ellipse's semi-axis (S_x and S_Y) of the fitted ellipse (naive approach) compared to the predicted ellipse (our prediction) for each frame of the whiteboard sequence presented in figure 9(a). In (b), we copy directly the result of specularity detection on the texture resulting in a mismatching in the intensity which is hard to blend with the texture. Moreover, this method is sensitive to the specularity detection quality and cannot predict future or new viewpoints.

which creates smooth but misplaced specularities. Moreover, in figures 12(a) and 12(b), local illumination models such as Phong's are unable to model accurately the shape and the intensity variation of the specularity. Using only point light sources, it is difficult to model extended light sources. A better rendering quality could be obtained by modeling the diffuse term. The simplicity of our method provides good results with room for improvement with additional parameters such as roughness.

7 LIMITATIONS

7.1 Mirror Surfaces and Non-Elliptical Specularities

In the case of a perfectly specular surface such a mirror, we cannot guarantee the elliptical shape of the specularity since light sources come in various shapes (particularly polygonal). We consider the general case of light bulbs and fluorescent lamps, which include

(a)

(b)

(c)

(d)
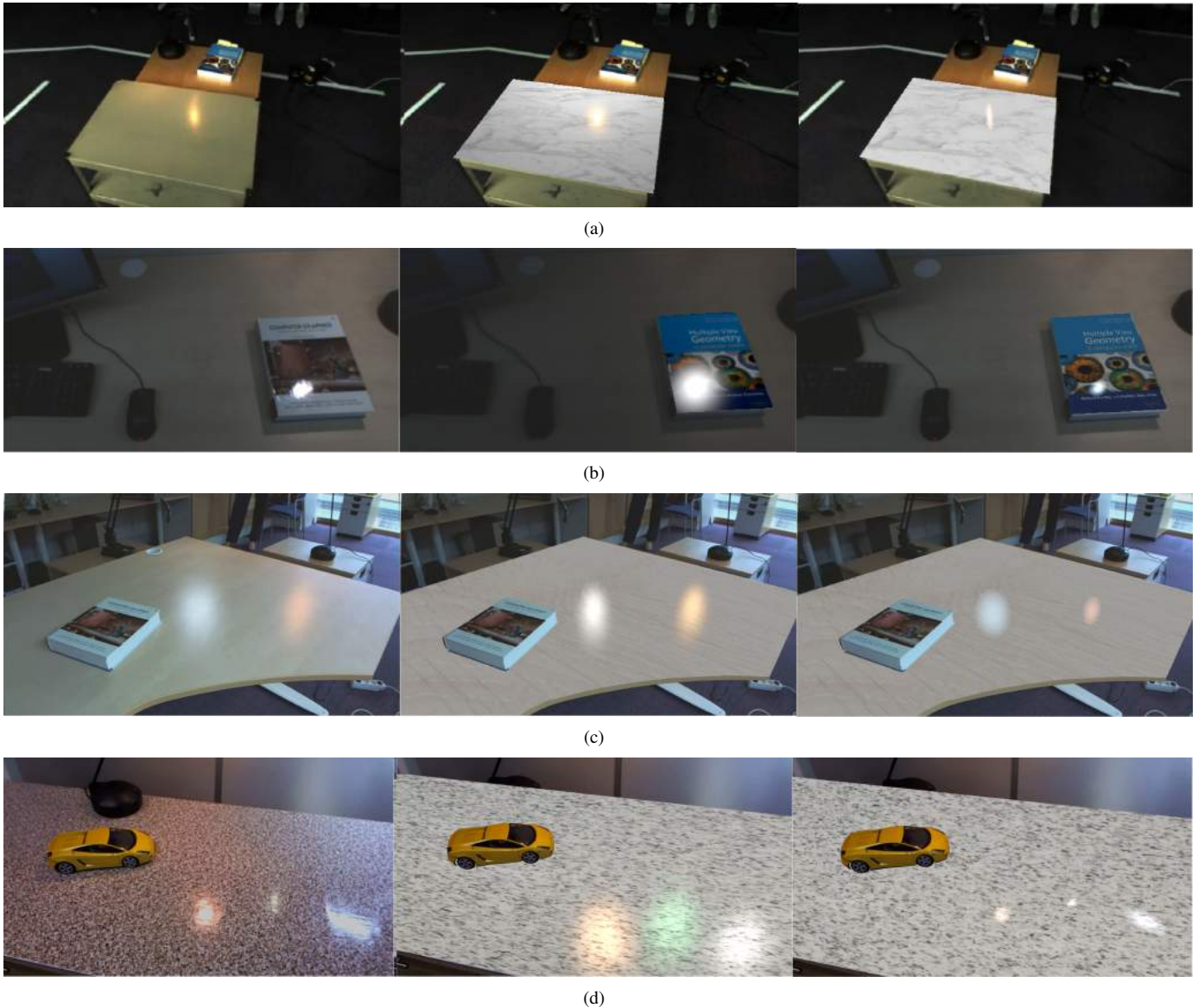
Figure 12: Comparison of retexturing methods for our implementation of [5] (middle) and our proposed approach (right). Since [5] is a recent method for point light source reconstruction, we manually added the roughness, the color and the intensity of the light source using a Phong illumination model. We only use the specular term. Retexturing is illustrated on the light bulb/steel table sequence (a) using a marble texture, (b) the light bulb/book sequence by switching the book cover, (c) the fluorescent lamp/light spot/wooden table sequence by changing the wooden texture of a table to another and (d) the multi-light/kitchen counter sequence using a rock texturing. To simulate the specularity, we used a Gaussian function and transformed it onto the plane surface using our specularity prediction to compute the transformation. The color of the specularity is computed from the specularities detected in the images used for the quadric reconstruction. Without considering the diffuse term on the texture, we can realistically change the texture of the planar surface using only the specular term predicted by JOLIMAS. As opposed to [5], we accurately match the shape, position and intensity of the specularity without relying on a known illumination model. Moreover, the computation of an illumination model such as Phong's cannot be done without priors on the materials and the number of light sources. The retextured sequences using our method can be found in the supplementary material.

most light sources found in an indoor context. Even with a slight roughness, our method will still be able to reconstruct a JOLIMAS model. The case of a mirror surface remains harder even for camera localization methods. An extension of our method using ideas such as in [17] would be interesting to study.

7.2 Influence of the Surface Roughness

In the case of surfaces with high roughness or bumpiness, since the surface normal varies a lot on a small surface (the surface remains planar as a whole), the specularity shape could vary from the initial conic shape. For retexturing, these variations are not included in our modeling of the specularity. It would be interesting to study the link between the specularity shape and the normal variations

of the surface such as in [2]. This is difficult due to the scale of the normal variations. Moreover, geometric modeling of the specularity is a novel idea.

7.3 Specularities Crossing

If the camera views a direction such that two light sources are close to alignment, two specularities could overlap in the image. They would defeat and fail the tracking and labeling of the specularities. Currently this issue is not handled in our framework but could be addressed if the lights are of different colors. However, for similar light sources (shape and color), the only way to clearly distinguish the specularities is to use 3D information (reconstruct a point light source from 2 viewpoints from instance) to ensure the coherence of the specularity's movement. In any case, the crossed specularities should not be used for reconstruction.

8 DISCUSSION AND CONCLUSION

We have presented a novel, geometric model for specularity prediction called JOint LIght-MAterial Specularity (JOLIMAS). After observing the conic shape of a specularity on a planar surface, a detailed demonstration on the Phong and Blinn-Phong reflection models was conducted to confirm the relevance of this approximation. We empirically validated this approximation for both point and extended light sources. In projective geometry a quadric projection generates a conic. By showing the existence of a fixed quadric whose projection is associated with a specularity on a viewpoint, we demonstrated a link between photometry (lights and materials) and multiple-view geometry (quadrics). The quadric is reconstructed from conics fitted to specularities. This model was tested on synthetic and real sequences for various light source types such as light bulbs and fluorescent lamps. The specularity prediction ability of our model allows us to detect changing states of the light sources (turned on and off) and achieves dynamic retexturing by changing the plane texture and rendering a specularity in a multi-lights context. We showed that JOLIMAS could be used to improve the realism of AR applications by rendering specularities. Moreover, specularity prediction could greatly improve camera localization algorithms. For computer graphics applications, the computation of the specular term could be quickly rendered using our predictions. We also plan to extend JOLIMAS to curved surfaces. This will require one to study how the surface's unflatness deforms the specularity's isocontours, as the specularity shape seems related to the second derivative of the surface [12]. A link could thus be found between JOLIMAS and surface curvature.

ACKNOWLEDGEMENT

APPENDIX A
VECTORIZATION OF THE DUAL QUADRIC PROJECTION SYSTEM

A detailed process of the vectorization of equation (10) can be found here. We define two vectorization operators, as in [18], vec for any matrix and vech for symmetric matrices such as $\mathtt{C}$, $\mathtt{Q}$:

$$\mathtt{X} = \begin{bmatrix} a & b \\ b & d \end{bmatrix}, \ \mathrm{vec}(\mathtt{X}) = \begin{bmatrix} a & b & b & d \end{bmatrix}^\top, \ \mathrm{vech}(\mathtt{X}) = \begin{bmatrix} a & b & d \end{bmatrix}^\top.$$

We apply vech to equation (10):

$$\mathrm{vech}(\Pi\mathtt{Q}^*\Pi^\top) = \mathrm{vech}(\mathtt{C}^*)$$

which can be rewritten as:

$$\mathtt{H}\,\mathrm{vec}(\Pi\mathtt{Q}^*\Pi^\top) = \mathbf{C}_v^*, \text{ with } \mathtt{H} = \begin{bmatrix} 1 & 0 & 0 & 0 & 0 & 0 & 0 & 0 & 0 \\ 0 & 0.5 & 0 & 0.5 & 0 & 0 & 0 & 0 & 0 \\ 0 & 0 & 0.5 & 0 & 0 & 0 & 0.5 & 0 & 0 \\ 0 & 0 & 0 & 0 & 1 & 0 & 0 & 0 & 0 \\ 0 & 0 & 0 & 0 & 0 & 0.5 & 0 & 0.5 & 0 \\ 0 & 0 & 0 & 0 & 0 & 0 & 0 & 0 & 1 \end{bmatrix},$$

with $\mathtt{H} \in \mathbb{R}^{6\times9}$ as $\mathrm{vech}(\mathtt{X}) = \mathtt{H}\,\mathrm{vec}(\mathtt{X})$. From [18], with three matrices $\mathtt{A}$, $\mathtt{B}$ and $\mathtt{C}$, $\mathrm{vec}(\mathtt{ABC}) = (\mathtt{C}^\top \otimes \mathtt{A})\,\mathrm{vec}(\mathtt{B})$ with $\otimes$ the Kronecker product. We further develop in:

$$\mathtt{H}(\Pi \otimes \Pi)\,\mathrm{vec}(\mathtt{Q}^*) = \mathbf{C}_v^*.$$

vec and vech are also linked such as $\mathrm{vec}(\mathtt{X}) = \mathtt{G}\,\mathrm{vech}(\mathtt{X})$ with $\mathtt{G} \in \mathbb{R}^{16\times10}$. Finally, we obtain the linearization:

$$\mathtt{H}(\Pi \otimes \Pi)\mathtt{G}\,\mathrm{vech}(\mathtt{Q}^*) = \mathbf{C}_v^* \tag{14}$$

with

$$\mathtt{G} = \begin{bmatrix} 1 & 0 & 0 & 0 & 0 & 0 & 0 & 0 & 0 & 0 & 0 & 0 & 0 & 0 & 0 & 0 \\ 0 & 1 & 0 & 0 & 1 & 0 & 0 & 0 & 0 & 0 & 0 & 0 & 0 & 0 & 0 & 0 \\ 0 & 0 & 1 & 0 & 0 & 0 & 0 & 0 & 1 & 0 & 0 & 0 & 0 & 0 & 0 & 0 \\ 0 & 0 & 0 & 1 & 0 & 0 & 0 & 0 & 0 & 0 & 0 & 0 & 1 & 0 & 0 & 0 \\ 0 & 0 & 0 & 0 & 0 & 1 & 0 & 0 & 0 & 0 & 0 & 0 & 0 & 0 & 0 & 0 \\ 0 & 0 & 0 & 0 & 0 & 0 & 1 & 0 & 0 & 1 & 0 & 1 & 0 & 0 & 0 & 0 \\ 0 & 0 & 0 & 0 & 0 & 0 & 0 & 1 & 0 & 0 & 0 & 0 & 0 & 1 & 0 & 0 \\ 0 & 0 & 0 & 0 & 0 & 0 & 0 & 0 & 0 & 0 & 1 & 0 & 0 & 0 & 0 & 0 \\ 0 & 0 & 0 & 0 & 0 & 0 & 0 & 0 & 0 & 0 & 0 & 1 & 0 & 0 & 1 & 0 \\ 0 & 0 & 0 & 0 & 0 & 0 & 0 & 0 & 0 & 0 & 0 & 0 & 0 & 0 & 0 & 1 \end{bmatrix}^\top,$$

which gives the final form $\mathtt{B}\mathtt{Q}_v^* = \mathbf{C}_v^*$ with $\mathtt{B} = \mathtt{H}(\Pi \otimes \Pi)\mathtt{G}$.

APPENDIX B
ANALYSIS OF SPECULAR HIGHLIGHT ISOCONTOURS UNDER THE PHONG AND BLINN-PHONG MODELS

We give further explanations on the isocontour analysis for a special case of the Phong model for $\tau = 0$ and an analysis of the isocontours for the Blinn-Phong model for $\tau = 0$.

B.1 The Blinn-Phong Model

The Blinn-Phong intensity function of a 3D surface point $\mathbf{P}$ is given by:

$$I(\mathbf{P}) = i_a k_a + i_d k_d (\hat{\mathbf{L}}(\mathbf{P}) \cdot \hat{\mathbf{N}}) + i_s k_s (\hat{\mathbf{N}} \cdot \hat{\mathbf{H}}(\mathbf{P}))^n, \tag{15}$$

with the half-way vector $\hat{\mathbf{H}}$:

$$\hat{\mathbf{H}} = \frac{\hat{\mathbf{L}}(\mathbf{P}) + \hat{\mathbf{V}}(\mathbf{P})}{||\hat{\mathbf{L}}(\mathbf{P}) + \hat{\mathbf{V}}(\mathbf{P})||}$$

The specular term is defined by:

$$I_s(\mathbf{P}) \propto \hat{\mathbf{N}}(\mathbf{P})^\top \frac{\hat{\mathbf{L}}(\mathbf{P}) + \hat{\mathbf{V}}(\mathbf{P})}{||\hat{\mathbf{L}}(\mathbf{P}) + \hat{\mathbf{V}}(\mathbf{P})||}, \tag{16}$$

We expand equation (16) as:

$$I_s(\mathbf{P}) \propto \hat{\mathbf{N}}(\mathbf{P})^\top \frac{\mu(\mathbf{L} - \mathbf{P}) + \mu(\mathbf{V} - \mathbf{P})}{||\mu(\mathbf{L} - \mathbf{P}) + \mu(\mathbf{V} - \mathbf{P})||}, \tag{17}$$

In the same manner as the Phong model, we want to analyze the isocontours of a specular highlight from equation (17).

B.2 Analysis of the Highlight's Outer Ring, $\tau = 0$ for the Blinn-Phong Model

We solve the equation for $\tau = 0$:

$$\hat{\mathbf{N}}(\mathbf{P})^\top \frac{\mu(\mathbf{L} - \mathbf{P}) + \mu(\mathbf{V} - \mathbf{P})}{||\mu(\mathbf{L} - \mathbf{P}) + \mu(\mathbf{V} - \mathbf{P})||} = 0.$$

By expanding and collecting the monomials of same degrees, we have:

$(d°4)$ $P_Z ||\mathbf{P}||^2$

$(d°3)$ $-2(L_Z P_Z ||\mathbf{P}||^2 - V_Z P_Z ||\mathbf{P}||^2 - \mathbf{P}^\top \mathbf{L} P_Z^2 + \mathbf{P}^\top \mathbf{V} P_Z^2)$

$(d°2)$ $4(L_Z P_Z \mathbf{P}^\top \mathbf{V} - V_Z P_Z \mathbf{P}^\top \mathbf{L}) +$
$\quad P_Z^2(||\mathbf{V}||^2 - ||\mathbf{L}||^2) + (L_Z^2 - V_Z^2)||\mathbf{P}||^2$

$(d°1)$ $2(V_Z P_Z ||\mathbf{L}||^2 - L_Z P_Z ||\mathbf{V}||^2 + V_Z^2 \mathbf{P}^\top \mathbf{L} - L_Z^2 \mathbf{P}^\top \mathbf{V})$

$(d°0)$ $L_Z^2 ||\mathbf{V}||^2 - V_Z^2 ||\mathbf{L}||^2$.

We note that, $\mathbf{P} = \begin{bmatrix} P_X & P_Y & P_Z \end{bmatrix}^\top$. With $P_Z = 0$, the degrees 4 and 3 vanish and:

$(d°2)$ $(L_Z^2 - V_Z^2)||\mathbf{P}||^2$

$(d°1)$ $2(V_Z^2 \mathbf{L}^\top - L_Z^2 \mathbf{V}^\top)\mathbf{P}$

$(d°0)$ $L_Z^2 ||\mathbf{V}||^2 - V_Z^2 ||\mathbf{L}||^2$.

The monomials can be factored in the following form:

$$\tilde{\mathbf{P}}^\top \mathsf{J} \tilde{\mathbf{P}} = 0, \tag{18}$$

where $\tilde{\mathbf{P}} = \begin{bmatrix} \mathbf{P} & 1 \end{bmatrix}^\top$ are the homogeneous coordinates of $\mathbf{P}$. Matrix $\mathsf{J} \in \mathbb{R}^{4\times4}$ is symmetric and defined by:

$$\mathsf{J} = \begin{bmatrix} L_Z^2 - V_Z^2 & (V_Z^2 \mathbf{L} - L_Z^2 \mathbf{V})^\top \\ V_Z^2 \mathbf{L} - L_Z^2 \mathbf{V} & L_Z^2 ||\mathbf{V}||^2 - V_Z^2 ||\mathbf{L}||^2. \end{bmatrix} \tag{19}$$

We define the orthographic projection on S as:

$$\mathtt{A} = \begin{bmatrix} 1 & 0 & 0 \\ 0 & 1 & 0 \\ 0 & 0 & 0 \\ 0 & 0 & 1 \end{bmatrix}.$$

The highlight's outer ring is thus given by the conic:

$$\mathtt{C} = \mathtt{A}^\top \mathsf{J} \mathtt{A} = \begin{bmatrix} L_Z^2 - V_Z^2 & (V_Z^2 \bar{\mathbf{L}} - L_Z^2 \bar{\mathbf{V}})^\top \\ V_Z^2 \bar{\mathbf{L}} - L_Z^2 \bar{\mathbf{V}} & L_Z^2 ||\mathbf{V}||^2 - V_Z^2 ||\mathbf{L}||^2 \end{bmatrix},$$

with $\bar{\mathbf{V}} = \begin{bmatrix} V_X & V_Y \end{bmatrix}^\top$ and $\bar{\mathbf{L}} = \begin{bmatrix} L_X & L_Y \end{bmatrix}^\top$ are the orthographic projection of $\mathbf{V}$ and $\mathbf{L}$ on S respectively. $\mathtt{C}$ represents a real circle.

B.3 Special Case, Analysis for $\tau = 1$ for The Phong Model

The study of $\tau = 1$ concerns the points of maximum intensity on the surface S. For the Phong model, this study is interesting because for $\tau = 1$, the terms of degrees 3 and 4 vanish. The remaining terms are:

$(d°2)$ $\mathbf{P}^\top [\mathbf{R} - \mathbf{V}]_\times^2 \mathbf{P}$

$(d°1)$ $2\mathbf{P}^\top [\mathbf{V} \times \mathbf{R}]_\times (\mathbf{V} - \mathbf{R})$

$(d°0)$ $(\mathbf{R}^\top \mathbf{V})^2 - \tau^2 ||\mathbf{R}||^2 ||\mathbf{V}||^2$.

They can be factored in the following form:

$$\tilde{\mathbf{P}}^\top \mathsf{J} \tilde{\mathbf{P}} = 0, \tag{20}$$

where $\tilde{\mathbf{P}} = \begin{bmatrix} \mathbf{P} & 1 \end{bmatrix}^\top$ are the homogeneous coordinates of $\mathbf{P}$. Matrix $\mathsf{J} \in \mathbb{R}^{4\times4}$ is symmetric and defined by:

$$\mathsf{J} = \begin{bmatrix} [\mathbf{R} - \mathbf{V}]_\times^2 & [\mathbf{V} \times \mathbf{R}]_\times (\mathbf{V} - \mathbf{R}) \\ ([\mathbf{V} \times \mathbf{R}]_\times (\mathbf{V} - \mathbf{R}))^\top & (\mathbf{R}^\top \mathbf{V})^2 - ||\mathbf{R}||^2 ||\mathbf{V}||^2 \end{bmatrix}$$

It thus represent a quadric, and $\hat{\mathbf{P}}$ lies at the intersection of this quadric with S. The leading (3×3) block of J is $[\mathbf{R} - \mathbf{V}]_\times^2$ and thus has rank 2. Therefore, $\mathrm{rank}(\mathsf{J}) \geq 2$. We show below that $\mathsf{Q}\tilde{\mathbf{R}} = \mathsf{Q}\tilde{\mathbf{V}} = 0$. This means $\mathrm{rank}(\mathsf{J}) \leq 2$ and thus that $\mathrm{rank}(\mathsf{J}) = 2$. This also means that J is semi-definite, either non-positive or non-negative. The way we constructed the polynomial, starting from a fraction $I_s = \frac{a}{b} = \tau = 1$, with $a \leq b$ implies $a - b \leq 0$ and thus that J is a point quadric representing the line containing $\mathbf{R}$ and $\mathbf{V}$. Its intersection with S then yields the expected solution for $\hat{\mathbf{P}}$.

Showing $\tilde{\mathbf{R}} \in \mathsf{J}^\perp$. We have the leading part as:

$$[\mathbf{R} - \mathbf{V}]_\times^2 \mathbf{R} + [\mathbf{V} \times \mathbf{R}]_\times (\mathbf{V} - \mathbf{R}).$$

The first term is expanded as:

$$[\mathbf{R} - \mathbf{V}]_\times [\mathbf{R} - \mathbf{V}]_\times \mathbf{R}$$
$$= [\mathbf{R} - \mathbf{V}]_\times [\mathbf{V}]_\times \mathbf{R}$$
$$= [\mathbf{V}]_\times^2 \mathbf{R} - [\mathbf{R}]_\times [\mathbf{V}]_\times \mathbf{R}$$
$$= \mathbf{V} \times (\mathbf{V} \times \mathbf{R}) - \mathbf{R} \times (\mathbf{V} \times \mathbf{R}).$$

The second term is expanded as:

$$(\mathbf{V} \times \mathbf{R}) \times \mathbf{R} - (\mathbf{V} \times \mathbf{R}) \times \mathbf{R} = -\mathbf{V} \times (\mathbf{V} \times \mathbf{R}) + \mathbf{R} \times (\mathbf{V} \times \mathbf{R}),$$

which sum to zero. The last element is:

$$(\mathbf{R} - \mathbf{V})^\top [\mathbf{V} \times \mathbf{R}]_\times \mathbf{R} + (\mathbf{R}^\top \mathbf{V})^2 - ||\mathbf{R}||^2 ||\mathbf{V}||^2.$$

The first term is expanded as:

$$(\mathbf{R} - \mathbf{V})^\top (\mathbf{R} \times (\mathbf{R} \times \mathbf{V})) = -\mathbf{V}^\top (\mathbf{R} \times (\mathbf{R} \times \mathbf{V})) = -\mathbf{V}^\top [\mathbf{R}]_\times^2 \mathbf{V}.$$

We saw that the second and third terms (the degree 0 coefficients of the polynomial) are also equal to $\mathbf{V}^\top [\mathbf{R}]_\times^2 \mathbf{V}$, which concludes.

REFERENCES

[1] Andrew Blake. Does the brain know the physics of specular reflection? *Nature*, 343(6254):165–168, 1990.

[2] Andrew Blake and Gavin Brelstaff. Geometry from specularities. In *International Conference on Computer Vision*, ICCV, 1988.

[3] James F Blinn. Models of light reflection for computer synthesized pictures. In *ACM SIGGRAPH Computer Graphics*, SIGGRAPH, 1977.

[4] Bastiaan J Boom, Sergio Orts-Escolano, Xin X Ning, Steven McDonagh, Peter Sandilands, and Robert B. Fisher. Point light source estimation based on scenes recorded by a rgb-d camera. In *British Machine Vision Conference*, BMVC, 2013.

[5] Paul-Emile Buteau and Hideo Saito. Retrieving lights positions using plane segmentation with diffuse illumination reinforced with specular component. In *International Symposium on Mixed and Augmented Reality*, ISMAR, 2015.

[6] Ju Yong Chang, Ramesh Raskar, and Amit Agrawal. 3d pose estimation and segmentation using specular cues. In *Computer Vision and Pattern Recognition*, CVPR, 2009.

[7] Robert L Cook and Kenneth E. Torrance. A reflectance model for computer graphics. *Transactions on Graphics*, 1(1):7–24, 1982.

[8] Geoffrey Cross and Andrew Zisserman. Quadric reconstruction from dual-space geometry. In *International Conference on Computer Vision*, ICCV, 1998.

[9] Michael Csongei, Liem Hoang, and Christian Sandor. Interactive near-field illumination for photorealistic augmented reality on mobile devices. In *Virtual Reality*, VR, 2014.

[10] Farshad Einabadi and Oliver Grau. Discrete light source estimation from light probes for photorealistic rendering. In *British Machine Vision Conference*, BMVC, 2015.

[11] Andrew W Fitzgibbon, Robert B Fisher, et al. A buyer's guide to conic fitting. *DAI Research paper*, 1996.

[12] Roland W Fleming, Antonio Torralba, and Edward H Adelson. Specular reflections and the perception of shape. *Journal of Vision*, 4(9):10, 2004.

[13] Lukas Gruber, Tobias Langlotz, Pradeep Sen, Tobias Hoherer, and Dieter Schmalstieg. Efficient and robust radiance transfer for probeless photorealistic augmented reality. In *Virtual Reality*, VR, 2014.

[14] Toshiya Hachisuka, Shinji Ogaki, and Henrik Wann Jensen. Progressive photon mapping. In *ACM Transactions on Graphics (TOG)*, volume 27, page 130, 2008.

[15] Eric Haines and Tomas Akenine-Moller. Real-time rendering. 2002.

[16] R. I. Hartley and A. Zisserman. *Multiple View Geometry in Computer Vision*. Cambridge University Press, ISBN: 0521540518, second edition, 2004.

[17] Eric Heitz, Jonathan Dupuy, Stephen Hill, and David Neubelt. Real-time polygonal-light shading with linearly transformed cosines. *Transactions on Graphics*, 35(4):41, 2016.

[18] Harold V Henderson and SR Searle. Vec and vech operators for matrices, with some uses in jacobians and multivariate statistics. *Canadian Journal of Statistics*, 7(1):65–81, 1979.

[19] Jan Herling and Wolfgang Broll. High-quality real-time video inpainting with pixmix. *Transactions on Visualization and Computer Graphics*, 20(6):866–879, 2014.

[20] Gary B Hughes and Mohcine Chraibi. Calculating ellipse overlap areas. *Computing and Visualization in Science*, 15(5):291–301, 2012.

[21] Sunil Hadap Inso Kweon Hyeongwoo Kim, Hailin Jin. Specular reflection separation using dark channel prior. CVPR, 2013.

[22] Jan Jachnik, Richard A. Newcombe, and Andrew J. Davison. Real-time surface light-field capture for augmentation of planar specular. In *International Symposium on Mixed and Augmented Reality*, ISMAR, 2012.

[23] Wojciech Jarosz, Matthias Zwicker, and Henrik Wann Jensen. The beam radiance estimate for volumetric photon mapping. SIGGRAPH, 2008.

[24] Masayuki Kanbara and Naokazu Yokoya. Real-time estimation of light source environment for photorealistic augmented reality. In *International Conference on Pattern Recognition*, ICPR, 2004.

[25] Norihiko Kawai, Tomokazu Sato, and Naokazu Yokoya. Diminished reality based on image inpainting considering background geometry. *Transactions on Visualization and Computer Graphics*, 2015.

[26] Sebastian B Knorr and Daniel Kurz. Real-time illumination estimation from faces for coherent rendering. In *International Symposium on Mixed and Augmented Reality*, ISMAR, 2014.

[27] Pascal Lagger and Pascal Fua. Using specularities to recover multiple light sources in the presence of texture. In *International Conference on Pattern Recognition*, ICPR, 2006.

[28] Pascal Lagger, Mathieu Salzmann, Vincent Lepetit, and Pascal Fua. 3d pose refinement from reflections. In *Computer Vision and Pattern Recognition*, CVPR, 2008.

[29] Clifford Lindsay and Emmanuel Agu. Automatic multi-light white balance using illumination gradients and color space projection. In *International Symposium on Visual Computing*, ISVC, 2014.

[30] Maxime Meilland, Christian Barat, and Andrew Comport. 3d high dynamic range dense visual slam and its application to real-time object re-lighting. In *International Symposium on Mixed and Augmented Reality*, ISMAR, 2013.

[31] Maxime Meilland, A Comport, Patrick Rives, and INRIA Sophia Antipolis Méditerranée. Real-time dense visual tracking under large lighting variations. In *British Machine Vision Conference*, BMVC, 2011.

[32] Alexandre Morgand and Mohamed Tamaazousti. Generic and real-time detection of specular reflections in images. In *8th International Joint Conference on Computer Vision, Imaging and Computer Graphics Theory and Applications*, VISAPP, 2014.

[33] Aaron Netz and Margarita Osadchy. Recognition using specular highlights. In *Computer Vision and Pattern Recognition*, CVPR, 2013.

[34] Aaron Netz and Margarita Osadchy. Recognition using specular highlights. *Pattern Analysis and Machine Intelligence*, 35(3):639–652, 2013.

[35] Bui Tuong Phong. Illumination for computer generated pictures. *Communications of the ACM*, 18(6):311–317, 1975.

[36] Leo Reyes and Eduardo Bayro-Corrochano. The projective reconstruction of points, lines, quadrics, plane conics and degenerate quadrics using uncalibrated cameras. *Image and Vision Computing*, 23(8):693–706, 2005.

[37] Kai Rohmer, Wolfgang Buschel, Raimund Dachselt, and Thorsten Grosch. Interactive near-field illumination for photorealistic augmented reality on mobile devices. In *International Symposium on Mixed and Augmented Reality*, ISMAR, 2014.

[38] Imari Sato, Yoichi Sato, and Katsushi Ikeuchi. Acquiring a radiance distribution to superimpose virtual objects onto a real scene. *Visualization and Computer Graphics, IEEE Transactions on*, 5(1):1–12, 1999.

[39] Silvio Savarese, Li Fei-Fei, and Pietro Perona. What do reflections tell us about the shape of a mirror? In *Proceedings of the 1st Symposium on Applied perception in graphics and visualization*, pages 115–118. ACM, 2004.

[40] Nitesh Shroff, Yuichi Taguchi, Oncel Tuzel, Ashok Veeraraghavan, Srikumar Ramalingam, and Haruhisa Okuda. Finding a needle in a specular haystack. In *International Conference on Robotics and Automation*, ICRA, 2011.

[41] Geraldo Silveira and Ezio Malis. Real-time visual tracking under arbitrary illumination changes. In *Computer Vision and Pattern Recognition*, CVPR, 2007.

[42] Peter Sturm and Pau Gargallo. Conic fitting using the geometric distance. In *Asian Conference on Computer Vision*, ACCV. 2007.

[43] Satoshi Suzuki and Keiichi Abe. Topological structural analysis of digitized binary images by border following. *Computer Vision, Graphics, and Image Processing*, 30(1):32–46, 1985.

[44] Mohamed Tamaazousti, Vincent Gay-Bellile, S Naudet Collette, Steve Bourgeois, and Michel Dhome. Nonlinear refinement of structure from motion reconstruction by taking advantage of a partial knowledge of the environment. In *Computer Vision and Pattern Recognition*, CVPR, 2011.

[45] Gregory J Ward. The radiance lighting simulation and rendering system. In *Special Interest Group on Computer Graphics and Interactive Techniques*, SIGGRAPH, 1994.

[46] Kwan-Yee K Wong, Dirk Schnieders, and Shuda Li. Recovering light directions and camera poses from a single sphere. In *European Conference on Computer Vision*, ECCV. 2008.

Alexandre Morgand is a PhD candidate of the Université Clermont Auvergne, in Clermont-Ferrand, France in partnership with the ENCOV research group at the Institut Pascal and the LVIC laboratory at CEA-LIST under the supervision of Professor Adrien Bartoli. He received his Master's Degree in computer science from the EPITA in Paris, France, in 2013. His research objectives are to model the light sources to improve the rendering of augmented reality applications.

Mohamed Tamaazousti received his Master's Degree in applied mathematical from the University of Orleans, France in 2009. He received the Ph.D. degree in computer vision from the University Blaise Pascal, Clermont-Ferrand, France in 2013. He is currently a permanent researcher in the LVIC laboratory at CEA LIST. His main research interests include structure from motion for rigid scenes, real time vision-based localization and reconstruction (SLAM) for autonomous system. He is also interested in augmented and diminished reality applications.

Adrien Bartoli has held the position of Professor of Computer Science at Université Clermont Auvergne since fall 2009 and is a member of Institut Universitaire de France since fall 2016. He leads the Endoscopy and Computer Vision (ENCOV) research group at Institut Pascal, CNRS, UCA and CHU de Clermont-Ferrand. His main research interests include image registration and Shape-from-X for rigid and deformable environments, and their application in computer-aided endoscopy.